Crustal velocity structure of the Cathaysia block from an active-source seismic profile between Wanzai and Hui'an in southeast China

Jiyan Lin[a,b,f], Tao Xu[a,g*], Huiteng Cai[c*], Qingtian Lü[d], Zhiming Bai[a], Yangfan Deng[e], Yongqian Zhang[d], Minfu Huang[a,f], José Badal[h], Xing Jin[c]

[a] *State Key Laboratory of Lithospheric Evolution, Institute of Geology and Geophysics, Chinese Academy of Sciences, Beijing 100029, China*
[b] *Geophysical Exploration Center, China Earthquake Administration, Zhengzhou 450002, China*
[c] *Earthquake Administration of Fujian Province, Fuzhou 350003, China*
[d] *Institute of Mineral Resources, Chinese Academy of Geological Sciences, Beijing 100037, China*
[e] *State Key Laboratory of Isotope Geochemistry, Guangzhou Institute of Geochemistry, Chinese Academy of Sciences, Guangzhou 510640, China*
[f] *University of Chinese Academy of Science, Beijing 100049, China*
[g] *CAS Center for Excellence in Tibetan Plateau Earth Sciences, Beijing 100101, China*
[h] *Physics of the Earth, Sciences B, University of Zaragoza, Pedro Cerbuna 12, Zaragoza 50009, Spain*

** Corresponding authors: xutao@mai.iggcas.ac.cn (Tao Xu), caihuiteng@126.com (Huiteng Cai)*

Abstract

With the purpose of exploring the widely distributed Mesozoic granitoids in southeast China and the related mineralization, we carried out a new 530-km-long seismic wide-angle reflection and refraction (WARR) profile along the transect Wanzai- Hui'an. Based on a previous exploration performed in 2012 and the analysis of this WARR profile, we have deduced a detailed P-wave velocity model of the crust and uppermost mantle. The main results are: (1) The crustal thickness is about 30 to 32 km beneath the Yangtze Block and West Cathaysia, and 29 to 30 km below the East Cathaysia Block, which represents a significant thinning with respect to the worldwide average thickness of shields and platforms. (2) The variation in seismic velocity between the upper crust and middle-lower crust in the Yangtze and Cathaysia blocks indicates that the Shaoxing-Jiangshan-Pingxiang Fault is the tectonic boundary between these two blocks, and that the Zhenghe-Dapu Fault is the tectonic boundary between the western and

eastern blocks of Cathaysia. (3) The middle crust exhibits a low P-wave velocity layer of 6.2 km/s below the Wuyishan Metallogenic Belt. This low velocity layer can be attributed to delamination during the Caledonian orogeny and the Yanshanian extension. (4) The middle-lower crust shows a lateral velocity variation from west to east in Cathaysia. The subduction of the Paleo-Pacific plate is believed to be the main reason for the extensional tectonic environment and magmatism during the Yanshanian (Jurassic-Cretaceous) period, leading to significant crustal and lithospheric thinning. The relatively high velocity in the middle-lower crust and widely disseminated Cretaceous volcanic rocks in East Cathaysia may be related to the slab rollback of the Paleo-Pacific plate in the late Yanshanian (Cretaceous) period.

Keywords: Wide-angle reflection and refraction; P-wave velocity structure; Tectonic boundaries; Cathaysia Block; Southeast China.

1. Introduction

Since the Neoproterozoic, the amalgamation of the Yangtze and the Cathaysia blocks formed the south China mainland whose easternmost part (Fig. 1) is characterized by the widely distributed Mesozoic granitoids and abundant mineral resources (Zhou et al., 2006; Li and Li, 2007; Mao et al., 2011; Wang et al., 2013; Mao et al., 2014). Granitoids can be classified into belts according to their age and distributions. For instance, Indosinian (251-205 Ma) granitoids scattered throughout western Cathaysia, outcropping in small areas and showing structures related to a collisional frame (Fig. 1). Granitoid-volcanic rocks of the Early Yanshanian (180-142 Ma) period distributed throughout western Cathaysia in zones parallel to the coastline, associated with the origin of the rift and the partial melting of the crust. Granitoid-volcanic rocks of the Late Yanshanian (142-67 Ma) period scattered throughout East Cathaysia, revealing a southeastward migration towards the ocean, with origin in deep mafic igneous protoliths in the middle-lower crust caused by underplating of basaltic magmas (Zhou et al., 2006). Therefore, the spatial and temporal distribution

of Mesozoic granitoid-volcanic rocks in SE China occurred in changing tectonic environments in the course of different geodynamic processes.

Many geodynamic models have been proposed to interpret the mechanism of the Mesozoic granitoids and the mineral resource deposits in South China (Li and Li, 2007; Lin et al., 2018). Generally, these models can be classified into two groups: flat-slab subduction (Li and Li, 2007) and multi-terrane interaction (Lin et al., 2018). The crustal thickness, as well as the distribution of P-wave velocity in the crust and uppermost mantle can provide tight constraints on the formation of granitoid rocks and evidence of deep geodynamic processes. In fact, several studies based on seismic tomography of SE China provide images of crustal and lithospheric structures at different scales. Results obtained from receiver functions and the H-κ stacking method show that the crustal thickness is about 38-46 km in the west of South China and 26-34 km in the east of South China (Ai et al., 2007; Li et al., 2013; Ye et al., 2013, 2014; Guo et al., 2019; Shen et al., 2019).). These same studies give and a Poisson's ratio ranging between 0.20 and 0.31. The lithospheric thickness is also much greater in the west of South China (about 190 km) and much smaller in the east of South China (less than 100 km), even 60-70 km in the southeast coast of South China. Results obtained from surface wave tomography (Wang et al., 2015; Shen et al., 2016; Li et al., 2018; Li et al., 2020; Peng et al., 2020) reveal that the crustal and lithospheric structure present a significant difference in the west of South China with respect to the east of South China. However, since the average resolution of the broad-band seismographs is greater than 10 km, despite these studies the fine structure of the crust does not seem to be adequately resolved.

In contrast, Wide Angle Reflection and Refraction (WARR) profile can provide a detailed P-wave velocity image of the crust and uppermost mantle. Several WARR profiles have been conducted in recent years (Deng et al., 2011; Zhang et al., 2013b; Li et al., 2015; Cai et al., 2016; Kuo et al., 2016). The results prove that the crustal thickness ranges from 35 km in the eastern Yangtze Block to 28 km in the Taiwan Strait and that the average crustal velocity is about 6.2 km/s in the Cathaysia Block. These WARR profiles emphasize different crustal P-wave velocities in the East and West

Cathaysia blocks, and relatively high velocity in the middle-lower crust beneath the East Cathaysia Block (Li et al., 2015; Cai et al., 2016; Kuo et al., 2016). However, these profiles focus mainly on the East Cathaysia block and the edge of the West Cathaysia block. In addition, WARR data on the structure of the crust in the Qinhang Metallogenic Belt (QMB) and the Wuyishan Metallogenic Belt (WMB) are lacking (Fig. 1), which are essential for understanding the regional dynamics.

In order to investigate the area of Mesozoic granitoids and the mineral resources in SE China, in this paper we review a previous WARR profile from Ninghua to Hui'an that was later completed with a new WARR profile from Wanzai to Yongchun (Fig. 1). We use the 2D ray tracing method and the RAYINVR inversion algorithm (Zelt and Smith, 1992) to model the crustal and uppermost mantle P-wave velocity structure of the QMB, WMB and East Cathaysia. Finally, we discuss the crustal and lithospheric thinning, crustal P-wave velocity characteristics, regional mineralization, and related tectonic evolution in SE China.

2. Tectonic setting

The Shaoxing-Jiangshan-Pingxiang fault (SJPF) divides the South China continent into the Yangtze Block to the northwest and the Cathaysia Block to the southeast (Fig., 1). The Yangtze Block contains an Archean-Paleoproterozoic crystalline basement while the Cathaysia Block is divided into two zones, West Cathaysia and East Cathaysia (Xu et al., 2007; Lin et al., 2018). The former block has a Precambrian basement and is affected by a major magmatic and metamorphic event during the Early Paleozoic, while the latter consists of a series of metasedimentary and metaplutonic rocks (Xu et al., 2007).

Southeast China experienced multi-stage intracontinental orogeny since the Neoproterozoic, resulting in the 1300-km-wide South China fold belt and widely distributed Mesozoic granitoids (Zhou et al., 2006; Li and Li, 2007; Wang et al., 2013). Two periods of tectono-magmatism are recognized since the Mesozoic in South China, the Indosinian (Triassic) magmatism and the Yanshanian (Jurassic-Cretaceous) magmatism. The Early Indosinian period is syn-collisional and was formed in a

compressional setting, while the Late Indosinian period is late-collisional and was formed in a locally extensional environment. The granitoid-volcanic rocks belonging to the Early Yanshanian are characteristic of rift-type intraplate magmatism, whereas the Late Yanshanian magmatism is likely active continental margin magmatism (Zhou et al., 2006).

The Qinhang Metallogenic Belt (QMB) and the Wuyishan Metallogenic Belt (WMB) are two important metallogenic belts in SE China (Fig., 1), which are rich in copper, tungsten, tin, etc. These two metallogenic belts experienced complex tectonism since the Neoproterozoic, but the primary mineral resources were formed during the Mesozoic period (Mao et al., 2011; Mao et al., 2014).

3. Wide-angle seismic data and phase analysis

3.1 Seismic data acquisition

In December 2018, the Institute of Geology and Geophysics, Chinese Academy of Sciences, with the support of the China Key National R&D Program, completed a previous WARR profile from Ninghua to Hui'an with a long-530-km NW-SE-trending WARR profile from Wanzai to Yongchun (Fig. 1). Four shots (red stars in Fig. 1) were fired along the profile at intervals of about 80-90 km. The explosive charge of each shot varied from 2000 kg to 2520 kg. Along the profile, 435 portable seismographs (blue triangles in Fig. 1) were deployed with an average interval of about 1.2 km. Previously, to study the deep tectonic structure of the SE margin in mainland China, the Fujian Province Earthquake Administration had conducted a 270-km-long WARR profile from Ninghua to Hui'an (Cai et al., 2016), from June to August 2012. On that occasion, five shots (yellow stars in Fig. 1) were fired and 160 portable seismographs (green triangles in Fig. 1) were deployed along the profile, with shot points and receivers spaced 50 to 98 km and 1.5 to 2.0 km apart, respectively. The two WARR profiles have the same NW-SE direction and an overlap distance of 195 km between Ninghua and Yongchun. In this paper, we combine these two profiles to obtain the crustal and uppermost mantle P-wave velocity structure along the Wanzai-Hui'an transect that covers a distance between the

two locations of approximately 620 km.

3.2 Seismic phases on the record sections

Travel times are picked on shot gathers using the interactive picking and plotting program ZPLOT. All record sections (Figs. 2-10; Figs. S1-S9) are filtered by a 2-10 Hz band-pass filter. Travel times are converted to a reduced timescale using a reduction velocity of 6.0 km/s, in order to emphasize the features of the crust. The recorded crustal and uppermost mantle seismic phases include the refracted phase in the upper crust (Pg), reflected phases in the crystalline crust (P1, P2), reflected phases from the Moho (PmP) and refractions in the uppermost mantle (Pn).

The Pg phase can be collected at offsets of about 0-130 km and has an apparent velocity between 5.8 and 6.1 km/s. The Pg reduced time ranges from 0.1 to 0.4 s, indicating a relatively thin sedimentary cover in SE China. Intracrustal reflected phases (P1, P2) can be recognized at offsets of 50-190 km; two groups of P1 and P2 phases can be picked beneath Yangtze and West Cathaysia, but only one group of P1 can be recognized beneath East Cathaysia. The intracrustal reflected phases are unfailingly weaker than the PmP wave, which implies a relatively low impedance contrast for the P wave. The PmP phase is clearly recorded at offsets of 50-240 km and generally show great amplitude in all record sections. PmP arrivals on the record sections of shot points Sp24 and Sp25 are earlier than in other sections, revealing that the Moho depth is shallower beneath East Cathaysia. The refracted Pn phase in the upper mantle appears at offsets of 120-270 km, and with an apparent velocity of 8.0-8.1 km/s.

3.3. Seismic data processing

The early Pg arrivals in the WARR record sections have the highest signal-to-noise ratio, which can be used to constrain the velocity pattern of the upper crust. In this paper, we use the 2D finite-difference inversion method (Vidale, 1988, 1990; Hole, 1992) to invert for the upper crust structure. This method is much faster than the two-point ray-tracing method and more robust for highly heterogeneous media. A total of 869

travel times of Pg were used to determine the velocity of the upper crust. The gridding size of the upper crust model is 0.5×0.5 km. To invert this model, we apply the back-projection method with a grid-spacing of 1.0×1.0 km. The final model was calculated after 30 iterations, which reduced the root-mean-square (RMS) traveltime residual from 0.12 s to 0.02 s.

To model the seismic velocity structure of the crust and upper mantle we use the 2D ray-tracing method and the RAYINVR inversion algorithm (Zelt and Smith, 1992). First, we use the 1D traveltime fitting method, which is a trial-and-error method, and the upper crust model provided by finite differences to construct an initial 2D velocity model of crust and upper mantle (Lin et al., 2020). Then, we use all recognized phases (Pg, P1, P2, PmP and Pn) to determine the final model by applying a layer-by-layer forward modeling technique and keeping the shallow nodes constant when modeling the deep layers. The velocity model is iteratively modified several times up to the RMS traveltime residuals approach the inherent uncertainty of the data, which is approximately 0.05 s for the Pg phase and 0.1 s for other phases. We use the largest possible number of data. Ray tracing details regarding individual seismic phases are given in Table 1, including RMS residuals close to the uncertainties of the data and normalized square chi (χ^2) values. Adjusting the travel times for all shots points reveals a good match between the observed and calculated times (Fig. 11a) and a dense and uniform ray coverage for the entire profile (Fig. 11b).

4. Seismic velocity structure of the crust and uppermost mantle

The final 2D velocity model (Fig. 12a) presents a laterally varying P-wave velocity in the crust and upper mantle, and a relatively smooth variation of the Moho depth. The crustal thickness is 30-32 km beneath the Yangtze Block and West Cathaysia, and slightly shallower (29-30 km) beneath East Cathaysia. The Bouguer gravity anomaly along the reference profile (Fig. 12b) also shows a gradual increase in East Cathaysia, which adjusts to the Moho depth (Fig. 12a). The average crustal velocity is 6.14-6.18 km/s beneath the Yangtze Block and West Cathaysia and 6.23-6.25 km/s beneath East

207 Cathaysia.

208 The upper crust reveals as a heterogeneous structure along the profile. The thickness
209 of the sedimentary cover is relatively thin (1.0-3.0 km), taking the contour line of 5.8
210 km/s as the basement of the sedimentary layer. There is jump of 4.5 to 5.8 km/s at the
211 bottom of this lid. Nevertheless, it is thicker at distance of 300-500 km than in other
212 survey transects. The P-wave velocity of the upper crust is 4.5-6.2 km/s. The C1
213 interface occurs at a depth of about 17 km. The P-wave velocity shows an abrupt change
214 beneath the SJPF and the Zhenghe-Dapu Fault (ZDF), so it can be affected by these two
215 faults.

216 The middle-lower crust in East Cathaysia shows higher P-wave velocity (6.4-6.8
217 km/s) than in the Yangtze Block and West Cathaysia (6.2-6.7 km/s). The C2 interface
218 reaches a depth of 25 km and separates the middle crust from the lower crust, although
219 this limit remains undefined beneath East Cathaysia. The velocity at 19-23 km depth
220 below the WMB is relatively lower (6.1 km/s) than in any other zone at the same depth.
221 The velocity of the uppermost mantle is 8.0-8.1 km/s, with hardly any differences
222 throughout the entire profile (Fig. 12a).
223

224 **5. Resolution tests**

225 We use the single parameter test (Nielsen and Thybo, 2009; Zelt, 1999) to analyze
226 the spatial resolution of the model. A single parameter (a depth node or velocity value)
227 was tested at a time. The maximum possible changes, either in depth or in velocity, can
228 be measured as long as they do not lead to poor ray coverage or unacceptable values of
229 RMS residuals and square chi. According to our analysis, the limits of the upper crust,
230 the mid-lower crust and the Moho are well defined with a maximum uncertainty of ±
231 0.9 km, ±1.3 km and ±1.2 km, respectively (Fig. 13a). Regarding the uncertainty in
232 seismic velocity, the variation ranges are ±0.02 km/s and ±0.10 km/s in the upper
233 crust, ±0.02 km/s and ±0.16 km/s in the middle-lower crust (Fig. 13b), which proves
234 that the results are quite accurate because of the dense ray coverage of the model.
235

6. Discussion

6.1 Comparison with other results

As a way of estimating the reliability of our results, below we compare them with those obtained by Cai et al. (2016) when studying the easternmost branch of the WARR profile, which runs from Ninghua to Hui'an (Fig. 1). The Moho depth determined by Cai et al. shows the same geometry (dashed line in Fig. 12a) that the boundary found by us at offsets of 320-560 km, except for a small-scale discrepancy at distances of 320-360 km, due to different ray coverage of the new Sp04 record section. Recently, Zhang et al. (2020) have obtained a three-dimensional model of the Moho depth based on receiver function analysis, and the result is a Moho (yellow circles in Fig. 12a) that matches well with ours, thus supporting the robustness of our model.

Comparison of our results with those of other profiles or seismic arrays deployed near our profile seems to confirm this first impression. The average crustal thickness obtained by Wei et al. (2016) reaches approximately 30.43 km in the Cathaysia Block and 31.2 km in its central part according to Han et al. (2019). Starting from WARR data, Li et al. (2015) also deduced a similar depth of 30-33 km for the Moho discontinuity beneath the Cathaysia Block, and a relatively low velocity layer at the depth of 22 km in the eastern part of West Cathaysia. Before, Zhang and Wang (2007) and Zhang et al. (2013b), from the analysis of a WARR profile in the NW-SE direction, obtained the Moho depth of 30-34 km beneath the Yangtze Block and Cathaysia Block, and a low velocity layer at the depth of 15-20 km, which are data consistent with ours. As in our case, the results of Li et al. (2015) and Cai et al. (2016) show a medium-lower crust with relatively high velocity beneath East Cathaysia, which is approximately 0.2 km/s higher than in West Cathaysia. Both WARR data and receiver functions reveal that the crustal thickness in the eastern band of the Yangtze Block and Cathaysia Block varies between 29 and 35 km and is gradually less from inland to shore.

6.2 Lithospheric and crustal thinning

Lithospheric and crustal thinning may provide some information about the deep

geodynamic processes. Previous geophysical results demonstrate that the lithospheric thickness in eastern China has evolved since the Mesozoic (Chen et al., 2008; Zhu et al. 2012; Deng and Levandowski, 2018). P and S receiver functions show that the lithospheric thickness beneath the Cathaysia Block is less than 100 km (Zhang et al., 2018), being only 60-70 km in East Cathaysia (Li et al., 2013; Ye et al., 2014). However, the lithosphere is thicker (approximately 190 km) west of the Yangtze Craton (Zhang et al., 2018). Likewise, the Moho depth also varies from 45-50 km in the West Yangtze Craton to about 30 km in the Cathaysia Block (Li et al., 2013; Ye et al., 2014), showing the same variation features with the lithosphere thickness. In addition, Rayleigh wave tomography (Wang et al., 2015; Shan et al., 2017) and joint inversion of receiver functions and surface wave dispersion (Li et al., 2018; Deng et al., 2019) also prove that the crust and lithosphere are significantly thinned in eastern China.

Geochemical results indicate a thick lithosphere (110-230 km) in South China corresponding to the Paleozoic period (Zheng et al., 2015), although a thinner lithosphere (less than 80 km) during the Late Mesozoic (Liu et al., 2012). North China came to have an ancient thick lithosphere (about 200 km) in the Archean period, which is characteristic of a craton, but later underwent extensive modification during the Late Mesozoic period (Zhu et al., 2011, 2012). Thus, both the eastern part of South China and North China Craton experienced significant destruction and thinning of the lithosphere. Meanwhile, crustal thickness in eastern China was also reduced to about 30 km (Li et al., 2013; Jia et al., 2014; Tian et al., 2014; Ye et al., 2014; Li et al., 2015; Cai et al., 2016) relative to the global average crustal thickness of shields and platforms, which is 41.5 km (Christensen and Mooney, 1995).

6.3 Main tectonic boundaries

The SJPF is considered as the boundary between the Yangtze and Cathaysia blocks (Li, 1992; Zhang et al., 2005). However, our results show some heterogeneity in the upper crust below this fault, but no significant changes in the middle and lower crust, which can be attributed to insufficient ray coverage of the Yangtze Block.

The ZDF divides the Cathaysia Block into two parts: the western part and the eastern part (Xu et al., 2007; Li et al., 2015; Cai et al., 2016). Unlike before, now the clear variation in velocity of the middle and lower crust on both sides of this fault (Fig. 12a) provides evidence that the ZDF can probably extend into the deep crust. However, age-based evidence of Zircon U-Pb, Hf data and structural data presented by Li et al., (2018) have led to propose that the boundary between the western and eastern Cathaysia blocks is not the ZDF, but the Fujian fault that is located about 50 km northwest of the former. Regardless of this proposal, considering the obvious velocity difference in the middle and lower crust, we think that the deep boundary between West and East Cathaysia is the ZDF.

6.4 Tectonic evolution in SE China

The velocity model shown in Fig. 12a is characterized by relatively low velocity (6.1 km/s) below the WMB and high velocity (6.4-6.8 km/s) in the middle-lower crust of East Cathaysia. Based on the regional tectonic activity, we believe that the low velocity may be the expression of a ductile shear zone (Zhang and Wang, 2007), which is related to delamination during the Late-Caledonian (Silurian) period and the extension of the lithosphere during the Yanshanian (Jurassic-Cretaceous) period. As for the relatively high velocity observed in the middle-lower crust of East Cathaysia, we believe that it can be attributed to the slab rollback of the Paleo-Pacific plate (Zhao et al., 2013; Li et al., 2014; Li et al., 2017), which injects mafic material into the middle-lower crust. Furthermore, magmatic underplating in East Cathaysia during the Late Yanshanian (Cretaceous) period might be the cause of the comparatively high velocity in the middle-lower crust, and also of the widely distributed Cretaceous volcanic rocks in East Cathaysia (Xu et al., 2007; Shu et al., 2009; Zhang et al., 2009; Lin et al., 2018).

Strictly speaking, we can only relate the quoted physical results to the geodynamic processes mentioned above. However, according to previous geological and geophysical studies (Zhou et al., 2006; Shu, 2012; Wang et al., 2013; Zhang et al., 2013a; Shu et al., 2015) and the crustal P-wave velocity structure shown in this paper, we can describe a

larger picture in relation to the tectonic evolution in SE China on a geological time scale (Fig. 14). Four stages can be distinguished, namely: Early-Middle Caledonian (Ordovician) period (Fig. 14a), Late Caledonian (Silurian) period (Fig. 14b), Early Yanshanian (Jurassic) period (Fig. 14c) and Late Yanshanian (Cretaceous) period (Fig. 14d). First, the Caledonian orogeny between West Cathaysia and East Cathaysia resulted in a crustal thickening (Wang et al., 2013). Second, after post-orogenic extension, the lower crust and lithosphere collapsed (Wang et al., 2013). Third, the Paleo-Pacific plate began its subduction underneath the Eurasian plate. Accompanying this subduction, the lithospheric mantle was heated up and the asthenosphere upwelling made the extensional tectonic framework continue (Zhou and Li, 2000; He and Xu, 2012; Liu et al., 2015). Under an extensional tectonic regime, the crust and lithosphere thinned. Finally, due to the ongoing extension, the subduction dip angle increased because of the slab rollback, and the dehydration of the subduced slab produced more adakitic and felsic melts, resulting in extensive underplating in the lower crust (Zhang et al., 2009; Zhao et al., 2013; Li et al., 2014; Li et al., 2017). We believe that the Paleo-Pacific plate subduction and slab rollback provide the environmental conditions for the emergence of Mesozoic granitoids and mineral resources in SE China.

7. Conclusions

Based on the interpretation of the 620-km-long wide-angle seismic profile between Wanzai and Hui'an across the Yangtze and Cathaysia Blocks, we propose the following conclusions:

(1) The crustal thickness throughout the eastern part of the Yangtze Block and the Cathaysia Block is about 29-32 km and shows a gradual thinning pattern from inland to shore.

(2) Our crustal velocity model shows that the ZDF is the boundary between the western and eastern blocks of Cathaysia, but only suggests that the SJPF is the boundary between the Yangtze Block and West Cathaysia.

(3) There is a low velocity zone at a depth of about 20 km below the WMB. We

speculate that it can be due to the existence of a ductile shear zone, as consequence of a delamination process during the Caledonian (Ordovician- Silurian) orogeny and the lithosphere extension during the Yanshanian (Jurassic- Cretaceous) period.

(4) The crust in the eastern Yangtze Block and the Cathaysia Block thins significantly, and the seismic velocity in the middle-lower crust is higher in East Cathaysia block, which can be attributed to underplating related to the rollback of the Paleo-Pacific plate during the Late Yanshanian (Cretaceous) period.

Declaration of Competing Interest

We declare that this paper has not been submitted elsewhere. There are no conflicts of interest.

Acknowledgements

We would like to thank the Geophysical Exploration Center of the China Earthquake Administration, for providing us with the field seismic to conduct this research work. We would also like to thank Prof. Laicheng Miao, Prof. Jiayong Yan and Dr. Yunhao Wei for their helpful discussions. We appreciate the help of Dr. Chenglong Wu in making the cartoon figure included here as the last graphic illustration. This study was funded by the National Key Research and Development Project of China (2016YFC0600201 and 2018YFC1503204) and the National Natural Science Foundation of China (41790461 and 41774097).

References

Ai Y., Chen Q., Zeng F., Hong X., Ye W., 2007. The crust and upper mantle structure beneath southeastern China. *Earth Planet. Sci. Lett.* 260, 549-563.

Cai H., Jin X., Wang S., Li P., Chen W., 2016. The crust structure and velocity structure characteristics beneath Ninghua-Datian-Hui'an. *Chinese J. Geophys.* 59(1), 157-168 (in Chinese).

Chen, L., Tao, W., Zhao, L., Zheng, T., 2008. Distinct lateral variation of lithospheric thickness in the northeastern North China craton. *Earth Planet. Sci. Lett.* 267 (1–2), 56-68.

Christensen, N. I., Mooney, W. D., 1995. Seismic velocity structure and composition of the continental crust: A global view. *J. Geophys. Res.* 100 (B7), 9761-9788.

Deng Y., Lin S., Fan W., Liu J., 2011. Crustal structure beneath South China revealed by deep seismic sounding and its dynamics implications. *Chinese J. Geophys*. 54(10), 2450-2574 (in Chinese).

Deng Y., Levandowski W., 2018. Lithospheric alteration, intraplate crustal deformation, and topography in eastern China. *Tectonics* 37, 4120-4134.

Deng Y., Li J., Peng T., Ma Q., Song X., Sun X., Shen Y., Fan W., 2019. Lithospheric structure in the Cathaysia block (South China) and its implication for the Late Mesozoic magmatism. *Phys. Earth Planet. Inter.* 291, 24-34.

Guo L., Gao R., Shi L., Huang Z., Ma Y., 2019. Crustal thickness and Poisson's ratios of South China revealed from joint inversion of receiver function and gravity data. *Earth Planet. Sci. Lett.* 510, 142-152.

Han R., Li Q., Xu Y., Zhang H., Chen H., Lang C., Wu Q., Wang X., 2019. Deep structure background and Poisson's ratio beneath the intersection zone of Nanling and Wuyi. *Chinese J. Geophys.* 62(7), 2477-2489 (in Chinese).

He Z., Xu X., 2012. Petrogenesis of the Late Yanshanian mantle-derived intrusions in southeastern China: Response to the geodynamics of paleo-Pacific plate subduction. *Chemical Geology* 328, 208–221.

Hole J., 1992. Nonlinear High-Resolution Three-Dimensional Seismic Travel Time Tomography. *J. Geophys. Res.* 97, 6553-6562.

Jia S., Wang F., Tian X., Duan Y., Zhang J., Liu B., Lin J., 2014. Crustal structure and tectonic study of North China Craton from a long deep seismic sounding profile, *Tectonophysics* 627, 48-56.

Kuo Y., Wang C., Hao K., Jin X., Cai H., Lin J., Wu F., Yen H., Huang B., Liang W., Okaya D., Brown L., 2016. Crustal structures from the Wuyi-Yunkai orogen to the Taiwan orogen: The onshore-offshore wide-angle seismic experiments of the TAIGER and ATSEE projects. *Tectonophysics* 692, 164-180.

Li H., Song X., Lü Q., Yang X., Deng Y., Ouyang L., Li J., Li X., Jiang G., 2018. Seismic imaging of lithosphere structure and upper mantle deformation beneath east-central China and their tectonic implications. *J. Geophys. Res.: Solid Earth*, 123, 2856-2870.

Li J., 1992. Study on structure and evolution of oceanic-continental lithosphere in southeast China. Sci. and Technol. Press of China, Beijing.

Li J., Sun X., Wang S., He L., Fan A., Zhang P., 2020. Crustal shear wave velocity structure near the Jiujishan area from seismic ambient noise tomography: Implications for tectonic evolution in South China. *Chinese J. Geophys.* 63(1), 184-195 (in Chinese).

Li J., Zhang Y., Dong S., Johnston S., 2014. Cretaceous tectonic evolution of South China: A preliminary synthesis. *Earth-Science Reviews*, 134, 98-136.

Li P., Jin X., Wang S., Cai H., 2015. Crustal velocity structure of the

Shaowu-Nanping-Pingtan transect through Fujian from deep seismic sounding-tectonic implications. *Science China: Earth Science* 45, 1757-1767 (in Chinese).

Li Q., Gao R., Wu F., Guan Y., Ye Z., Liu Q., Hao K., He R., Li W., Shen X., 2013. Seismic structure in the southeastern China using teleseismic receiver functions. *Tectonophysics* 606, 24-35.

Li S., Zang Y., Wang P., Suo Y., Li X., Liu X., Zhou Z., Liu X., Wang Q., 2017. Mesozoic tectonic transition in South China and initiation of Paleo-Pacific subduction. *Earth Science Frontiers* 24(4), 213-225 (in Chinese).

Li Z., Li X., 2007. Formation of the 1300-km-wide intracontinental orogen and postorogenic magmatic province in Mesozoic South China: A flat-slab subduction model. *Geology* 35(2), 179-182.

Lin J., Tang G., Xu T., Cai H., Lü Q., Bai Z., Deng Y., Huang M., Jin X., 2020. P-wave velocity structure in upper crust and crystalline basement of the Qinhang and Wuyishan Metallogenic belt: constraint from the Wanzai-Hui'an deep seismic sounding profile. *Chinese J. Geophys.* 63(12), doi:10.6038/cjg2020O0158 (in Chinese).

Lin S., Xing G., Davis D., Yin C., Wu M., Li L., Jiang Y., Chen Z., 2018. Appalachian-style multi-terrane Wilson cycle model for the assembly of South China. *Geology* 46(4), 319-322.

Liu C., Liu Z., Wu F., Chu Z., 2012. Mesozoic accretion of juvenile sub-continental lithospheric mantle beneath South China and its implications: geochemical and re-Os isotopic results from Ningyuan mantle xenoliths. *Chemical Geology* 291, 186-198.

Liu L., Xu X., Xia Y., 2015. Asynchronizing paleo-Pacific slab rollback beneath SE China: Insights from the episodic Late Mesozoic volcanism. *Gondwana Research* 37, 397-407.

Mao J., Chen M., Yuan S., Guo C., 2011. Geological characteristics of the Qinhang (or Shihang) metallogenic belt in South China and spatial-temporal distribution regularity of mineral desposits. *Atca Seismologica Sinica* 85(5), 636-658 (in Chinese).

Mao J., Li Z., Ye H., 2014. Mesozoic tectono-magmatic activities in South China: Retrospect and prospect. *Science China: Earth Sciences* 44(12): 2593-2617 (in Chinese).

Nielsen C., Thybo H., 2009. No Moho uplift below the Baikal Rift Zone: Evidence from a seismic refraction profile across southern Lake Baikal. *J. Geophys. Res.: Solid Earth* 114, B08306.

Peng J., Huang J., Liu Z., Xing K., 2020. Constraints on S-wave velocity structures of the lithosphere in mainland China from broadband ambient noise tomography. *Phys. Earth Planet. Inter.* 299, 106406.

Shan B., Xiong X., Zhao K., Xie Z., Zheng Y., Zhou L., 2017. Crustal and upper-mantle structure of South China from Rayleigh wave tomography. *Geophys. J. Int.* 208,

462 1643-1654.

463 Shen W., Ritzwoller M., Kang D., Kim Y., Lin F., Ning J., Wang W., Zheng Y., Zhou L.,
464 2016. A seismic reference model for the crust and uppermost mantle beneath China
465 from surface wave dispersion. *Geophys. J. Int.*, 206, 954-979.

466 Shen X., Kind R., Huang Z., Yuan X., Liu M., 2019. Imaging the Mantle Lithosphere
467 below the China cratons using S-to-p converted waves. *Tectonophysics* 754: 73-79.

468 Shu L., 2012. An analysis of principal features of tectonic evolution in South China
469 Block. *Geological Bulletin of China* 31 (7),1035-1053 (in Chinese).

470 Shu L., Wang B., Cawood P., Santosh M., Xu Z., 2015. Early Paleozoic and Early
471 Mesozoic intraplate tectonic and magmatic events in the Cathaysia Block, South
472 China. *Tectonics* 34, 1600–1621.

473 Shu L., Zhou X., Deng P., Wang B., Jiang S., Zhao X., 2009. Mesozoic tectonic
474 evolution of the Southeast China Block: New insights from basin analysis. *Jour. Asian*
475 *Earth Sci.* 34, 376-391.

476 Tian X., Zelt C., Wang F., Jia S., Liu Q., 2014. Crust structure of the North China Craton
477 from a long-range seismic wide-angle-reflection/refraction data. *Tectonophysics* 634,
478 237-245.

479 Vidale, J.E., 1988. Finite-difference calculation of travel times. *Bull. Seismol. Soc. Am.*
480 78, 2062-2076.

481 Vidale, J.E., 1990. Finite-difference calculation of traveltimes in three dimensions.
482 *Geophysics* 55, 521-526.

483 Wang M., Chen Y., Liang X., Xu Y., Fan Y., Xu T., Zhang Z., Teng J., 2015. Surface
484 wave tomography for South China and the northern South China Sea area. *Chinese J.*
485 *Geophys.* 58(6), 1963-1975 (in Chinese).

486 Wang Y., Zhang A., Fan W., Zhang Y., Zhang Y., 2013. Origin of
487 paleosubduction-modified mantle for Silurian gabbro in the Cathaysia Block:
488 Geochronological and geochemical evidence. *Lithos* 160-161, 37-54.

489 Wei Z., Chen L., Li Z., Ling Y., Li J., 2016. Regional variation in Moho depth and
490 Poisson's ratio beneath eastern China and its tectonic implications. *Jour. Asian Earth*
491 *Sci.* 115, 308-320.

492 Xu X., O'Reilly S., Griffin W., Wang X., Pearson N., He Z., 2007. The crust of
493 Cathaysia: Age, assembly and reworking of two terranes. *Precambrian Research* 158,
494 51–78.

495 Ye Z., Li Q., Gao R., Guan Y., He R., Wang H., Lu Z., Xiong X., Li W., 2013. Seismic
496 receiver functions revealing crust and upper mantle structure beneath the continental
497 margin of southeastern China. *Chinese J. Geophys.* 56(9), 2947-2958 (in Chinese).

498 Ye Z., Li Q., Gao R., Zhang H., He R., Wang H., Li W., 2014. A thinned lithosphere
499 beneath coastal area of southeastern China as evidenced by seismic receiver functions.
500 *Science China: Earth Sciences* 57, 2835–2844 (in Chinese).

Zelt C.A., 1999. Modelling strategies and model assessment for wide-angle seismic traveltime data. *Geophys. J. Int.* 139, 183-204.

Zelt C.A., Smith R.B., 1992. Seismic traveltime inversion for 2-D crustal velocity structure. *Geophys. J. Int.* 108, 16-34.

Zhang G., Guo A., Wang Y., Li S., Dong Y., Liu S., He D., Cheng S., Lu R., Yao A., 2013a. Tectonics of South China continent and its implications. *Science China: Earth Sciences* 56, 1804-1828 (in Chinese).

Zhang J., Zheng Y., Zhao Z., 2009. Geochemical evidence for interaction between oceanic crust and lithospheric mantle in the origin of Cenozoic continental basalts in east-central China. *Lithos* 110, 305-326.

Zhang Y., 2020. The Moho variation and crustal composition of South China: implication for the geological setting and metallogenesis. *Ore Geology Reviews*, submitted.

Zhang Y., Chen L., Ai Y., Jiang M., Xu W., Shen Z., 2018. Lithospheric structure of the South China Block from S-receiver function. *Chinese J. Geophys.* 61, 138-149 (in Chinese).

Zhang Z., Badal J., Li Y., Chen Y., Yang L., Teng J., 2005. Crust-upper mantle seismic velocity structure across southeastern China. *Tectonophysics* 395(1), 137-157.

Zhang Z., Wang Y., 2007. Crustal structure and contact relationship revealed from deep seismic sounding data in South China. *Phys. Earth Planet. Inter.* 165, 114-126.

Zhang Z., Xu T., Zhao B., Badal J., 2013b. Systematic variations in seismic velocity and reflection in the crust of Cathaysia: New constraints on intraplate orogeny in the South China continent. *Gondwana Research* 24, 902-917.

Zhao Z., Dai L. Zheng Y., 2013. Postcollisional mafic igneous rocks record crust-mantle interaction during continental deep subduction. *Nature: Scientific Reports* 3, 3413.

Zheng J., Lee C., Lu J., Zhao J. Wu Y., Xia B., Li X., Zhang J., Liu Y., 2015. Refertilization-driven destabilization of subcontinental mantle and the importance of initial lithospheric thickness for the fate of continents. *Earth Planet. Sci. Lett.* 409, 225-231.

Zhou X., Li W., 2000. Origin of Late Mesozoic igneous rocks in southeastern China: Implications for lithosphere subduction and underplating of mafic magmas. *Tectonophysics*, 326(3-4), 269–287.

Zhou X., Sun T., Shen W., Shu L., Niu Y., 2006. Petrogenesis of Mesozoic granitoids and volcanic rocks in South China: A response to tectonic evolution. *Episodes* 29(1), 26-33.

Zhu R., Chen L., Wu F., Liu J., 2011. Timing, scale and mechanism of the destruction of the North China Craton. *Sci. China Earth Sci.* 2011(54), 789-797 (in Chinese).

Zhu R., Xu Y., Zhu G., Zhang H., Xia Q., Zheng T., 2012. Destruction of the North China Craton. *Sci. China Earth Sci.* 2012(42), 1135-1159 (in Chinese).

540

Table 1. Ray tracing details for individual seismic phases.

Seismic phase	Total number of picks	Number of modelled picks	Percentage of picks	RMS (s)	χ^2
Pg	869	854	98.3%	0.066	1.756
P1	229	229	100.0%	0.084	0.713
P2	200	200	100.0%	0.092	0.856
PmP	767	755	98.4%	0.132	1.757
Pn	240	225	93.7%	0.132	1.749

Figures and legends

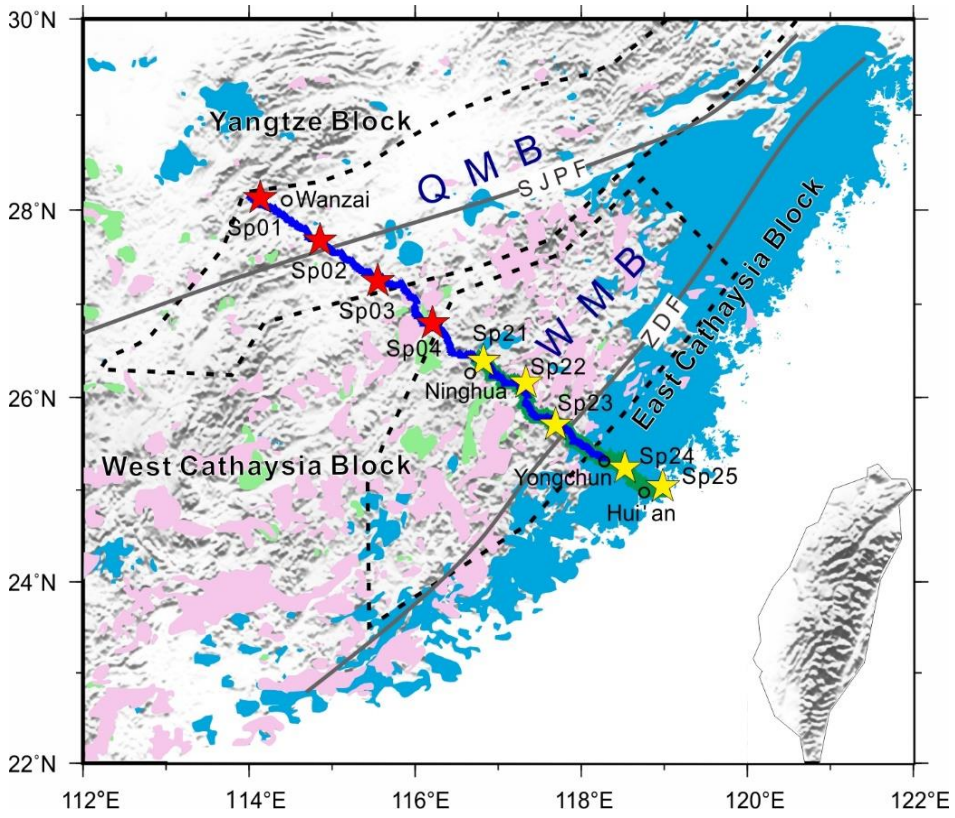

Figure 1. Map showing the location of the deep seismic sounding profile and geological structure. Red and yellow stars represent shot points, while blue and green triangles indicate short period seismic stations. Igneous rocks (after Zhou et al., 2006): light green areas represent Indosinian granites; pink areas show Early Yanshanian granitoid-volcanic rocks; light blue areas are Late Yanshanian granitoid-volcanic rocks. Faults: SJPF, Shaoxing-Jiangshan-Pingxiang fault; ZDF, Zhenghe-Dapu fault. Metallogenic Belts: QMB, Qinhang Metallogenic Belt; WMB, the Wuyishan Metallogenic Belt.

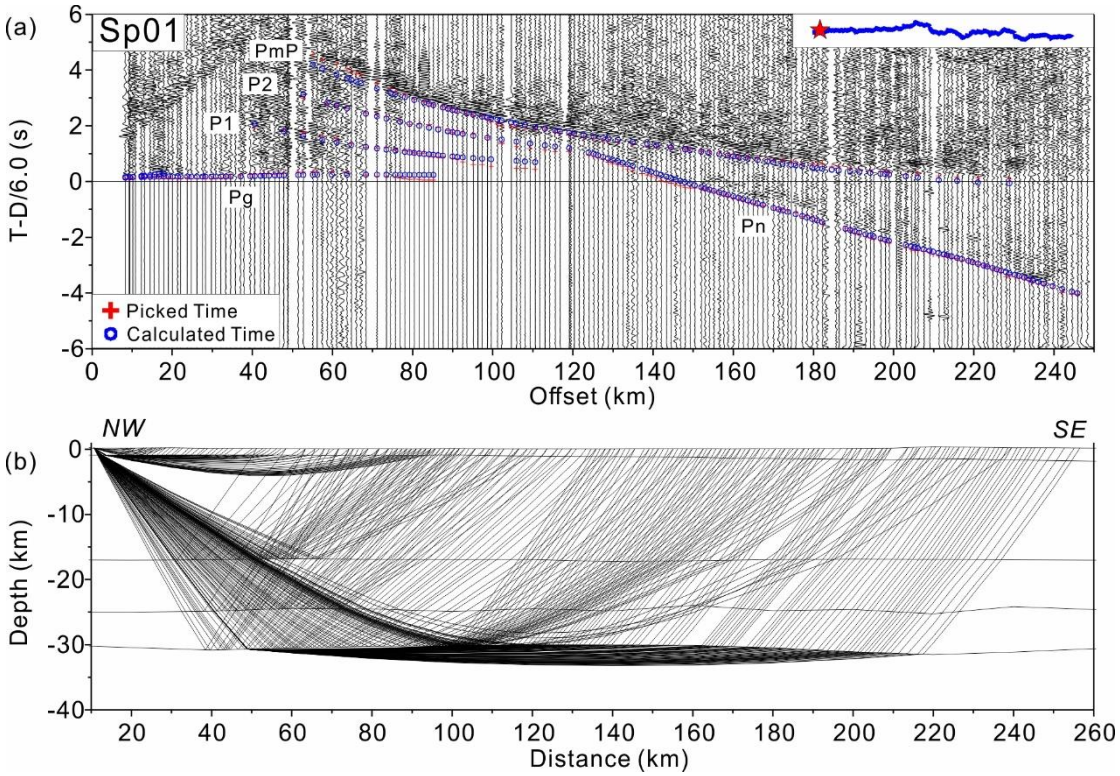

Figure 2. (a) P-wave record section (on a reduced time scale with a reduction velocity of 6.0 km/s) corresponding to the shot point Sp01 and identified seismic phases. Red crosses and blue circles indicate picked times and calculated times, respectively. (b) Ray tracing diagram.

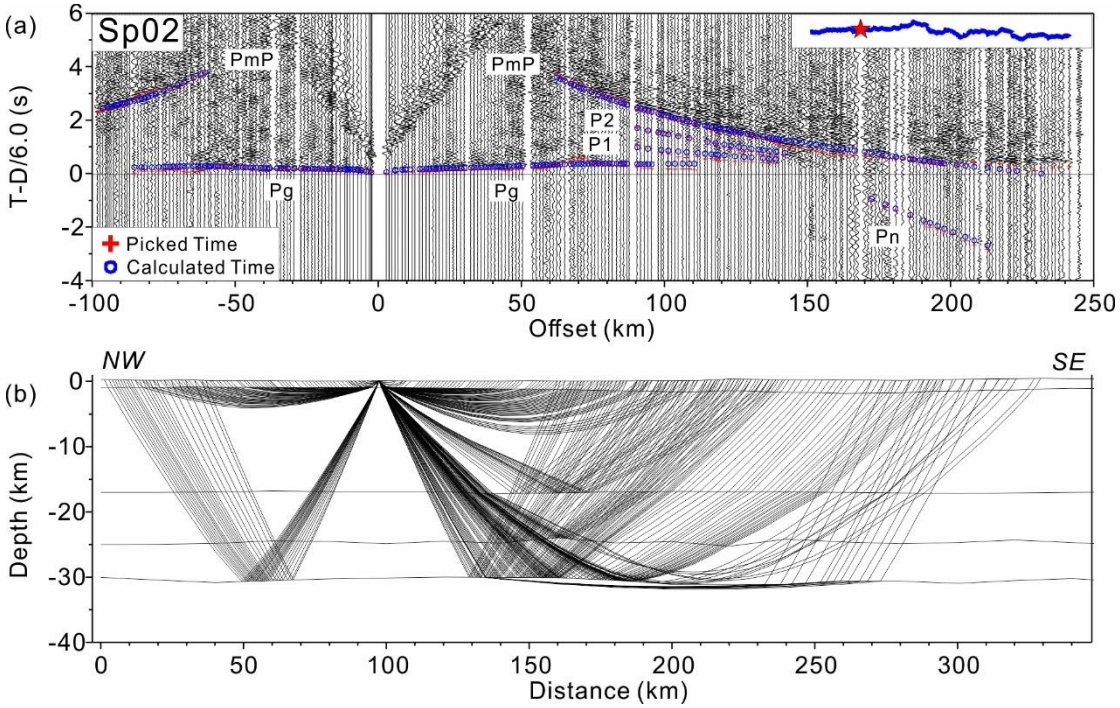

Figure 3. Same as in Fig. 2 for shot point Sp02.

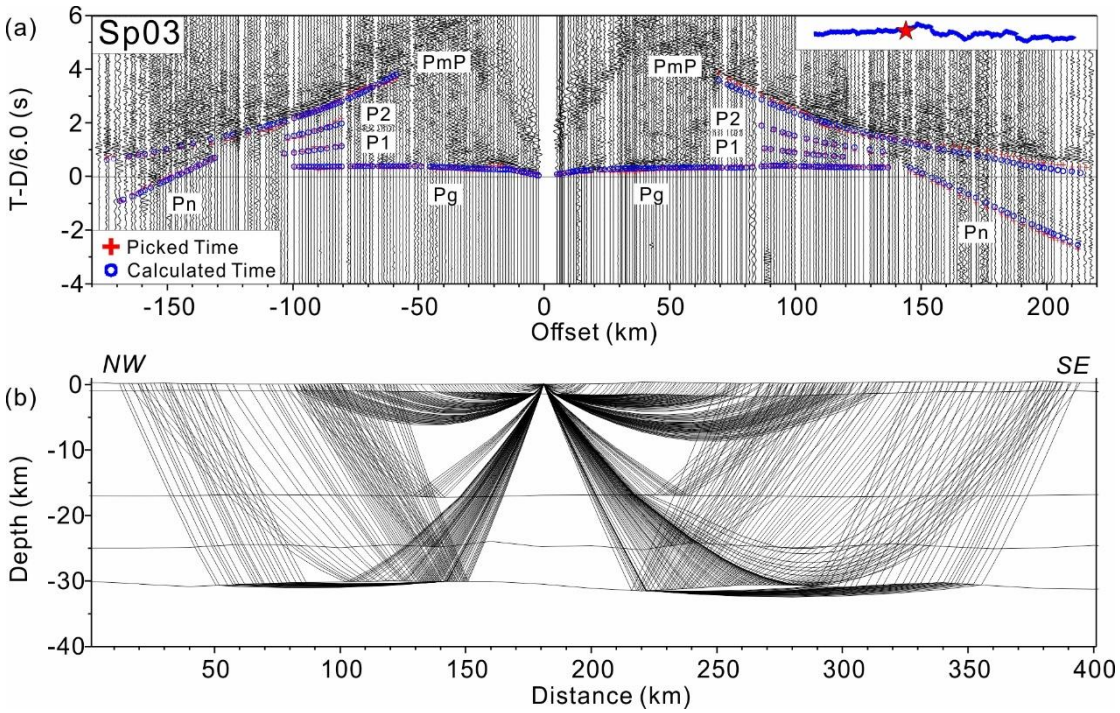

564

565 Figure 4. Same as in Fig. 2 for shot point Sp03.

566

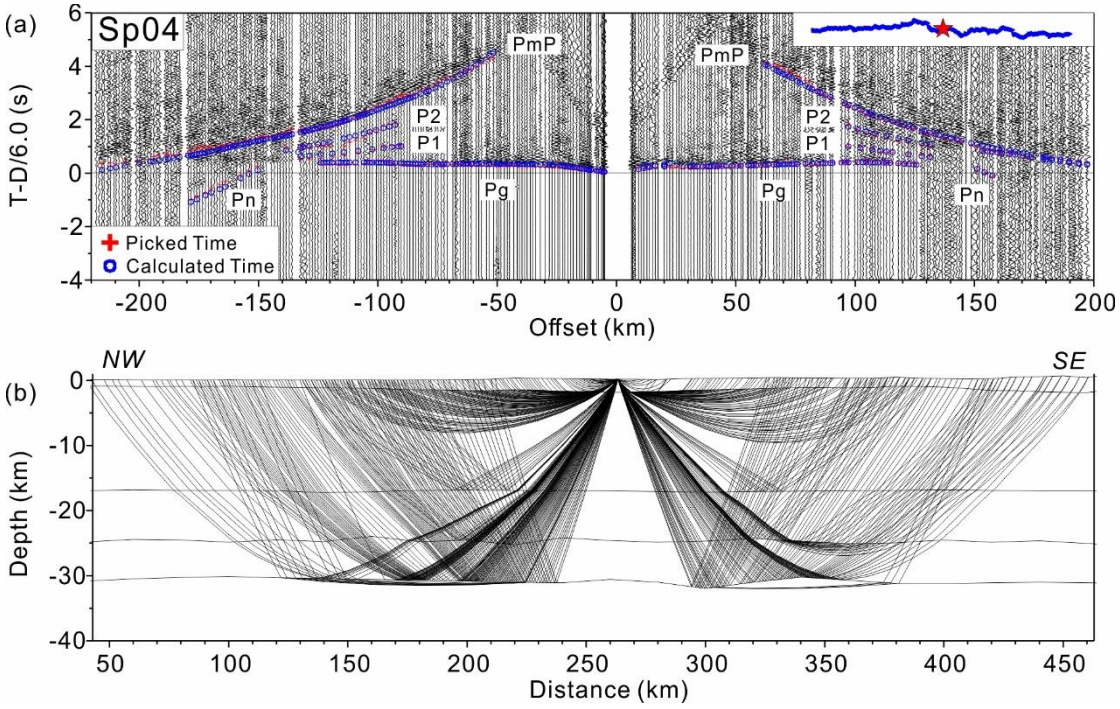

567

568 Figure 5. Same as in Fig. 2 for shot point Sp04.

569

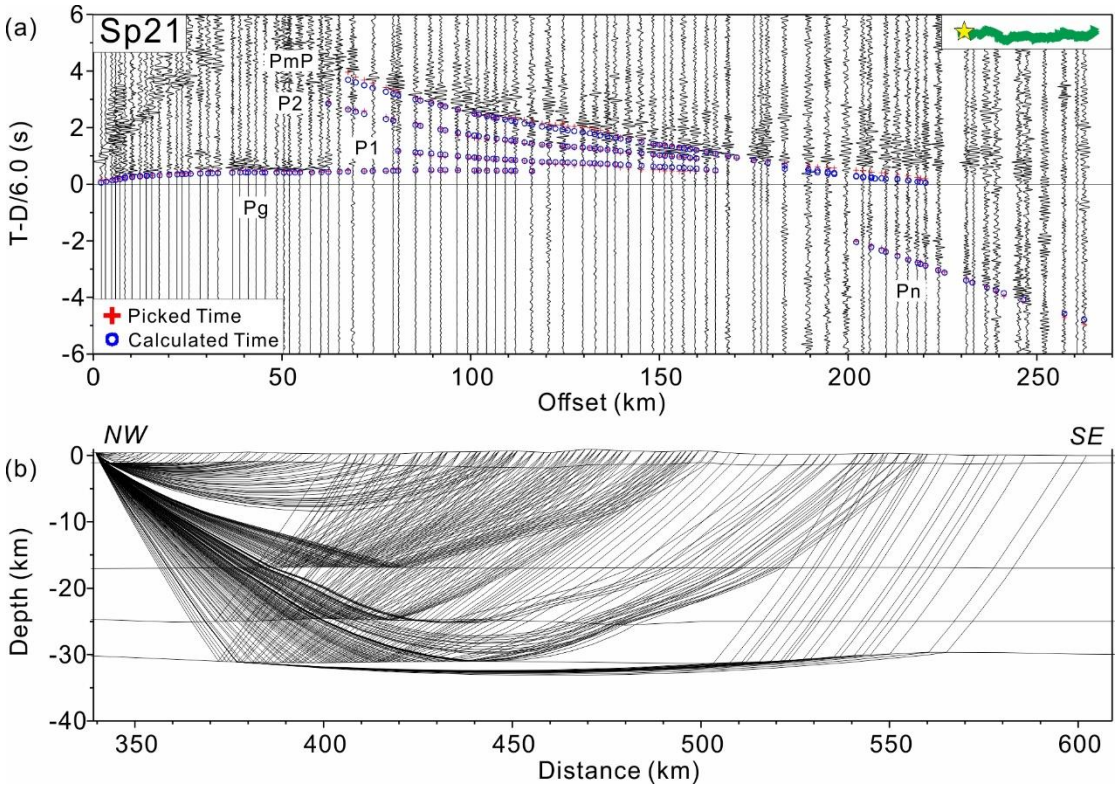

570

571 Figure 6. Same as in Fig. 2 for shot point Sp21.

572

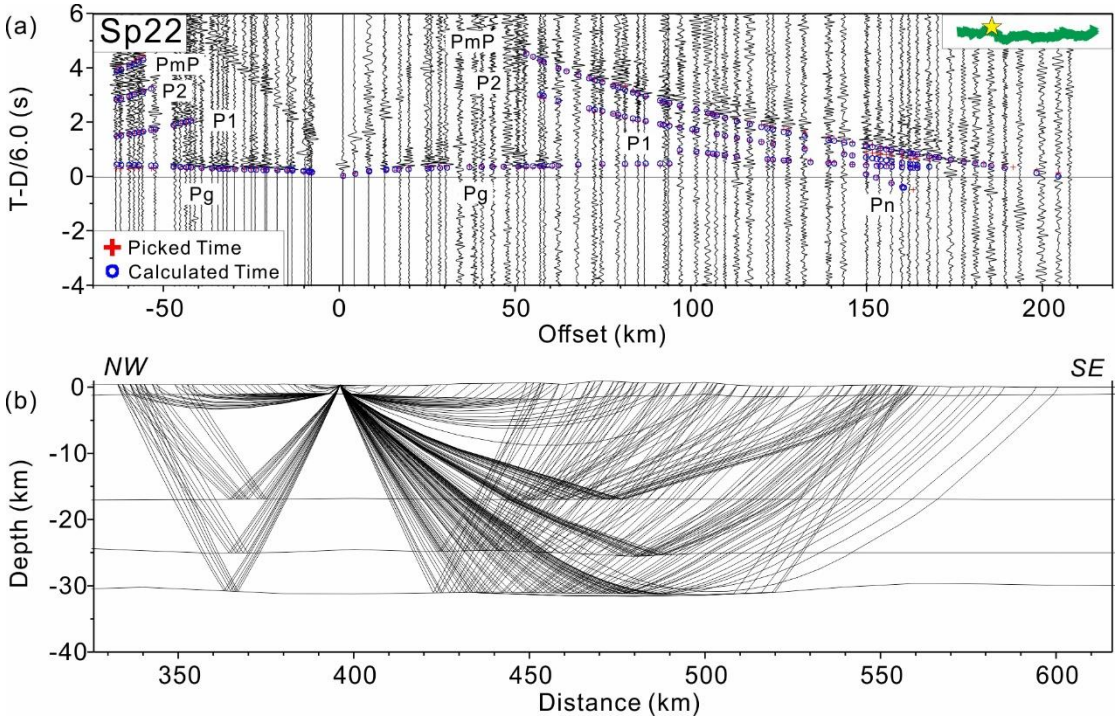

573

574 Figure 7. Same as in Fig. 2 for shot point Sp22.

575

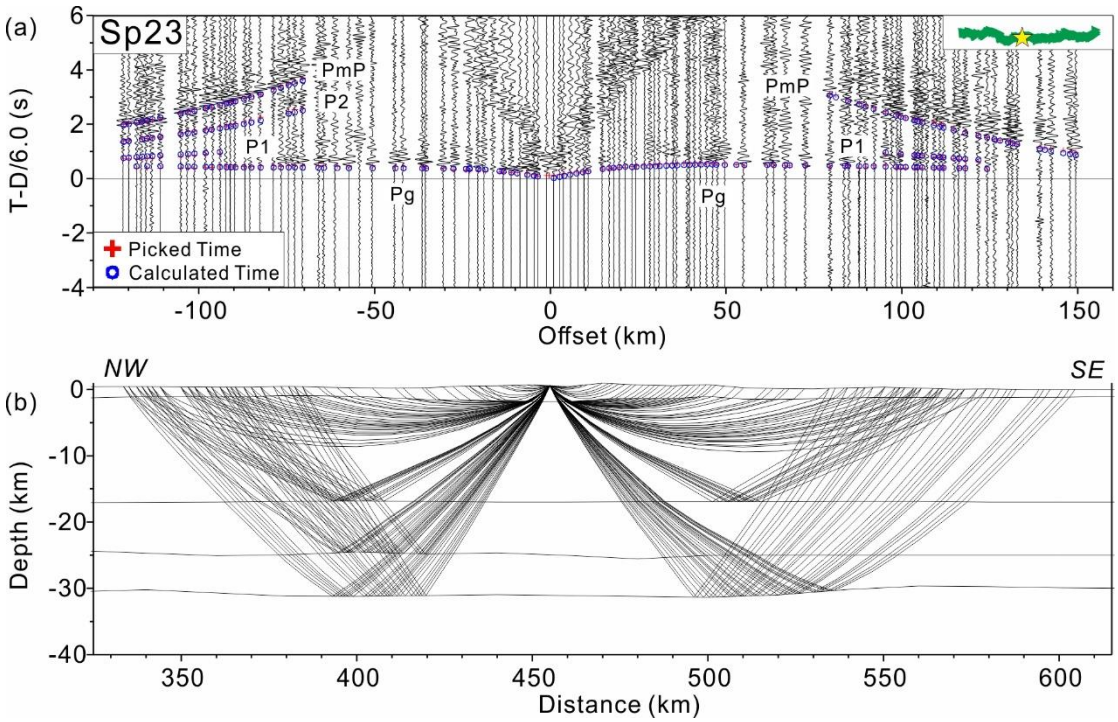

576

577 Figure 8. Same as in Fig. 2 for shot point Sp23.

578

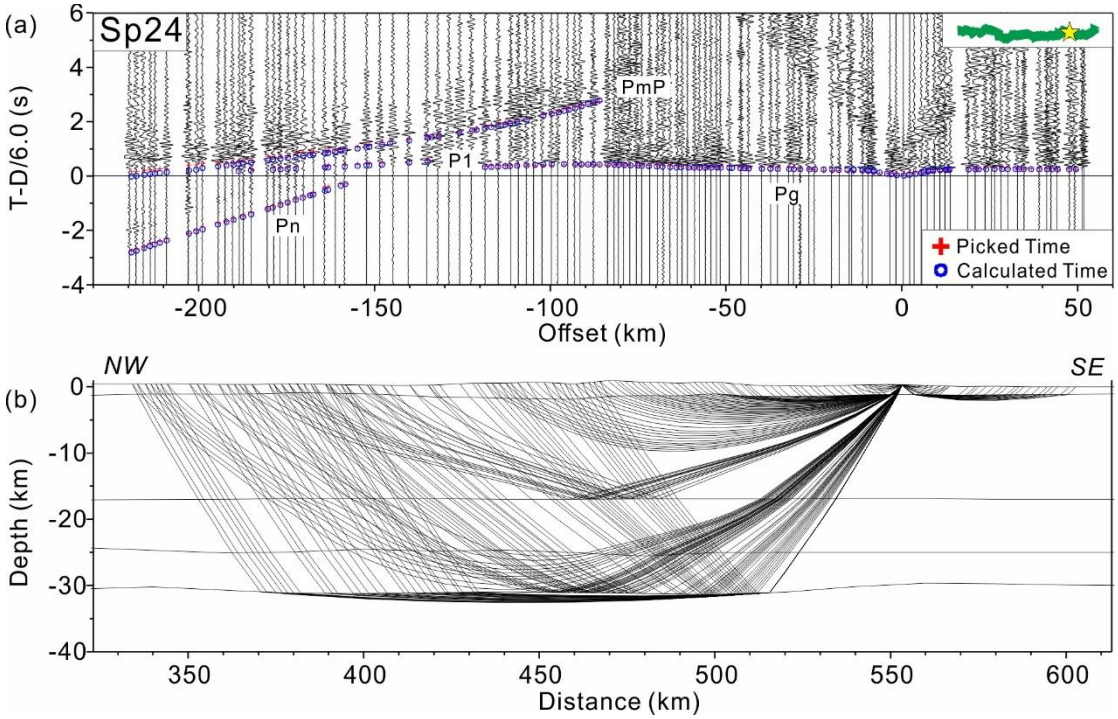

579

580 Figure 9. Same as in Fig. 2 for shot point Sp24.

581

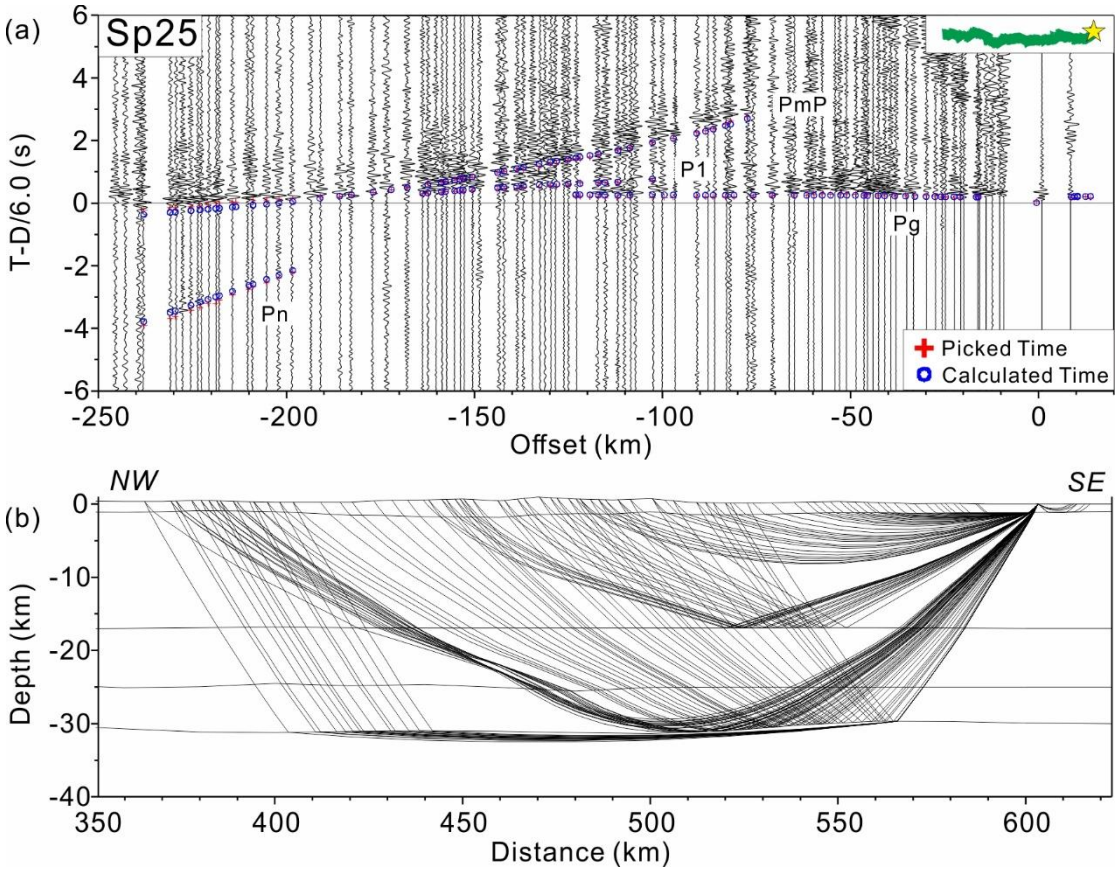

582

583 Figure 10. Same as in Fig. 2 for shot point Sp25.

584

585

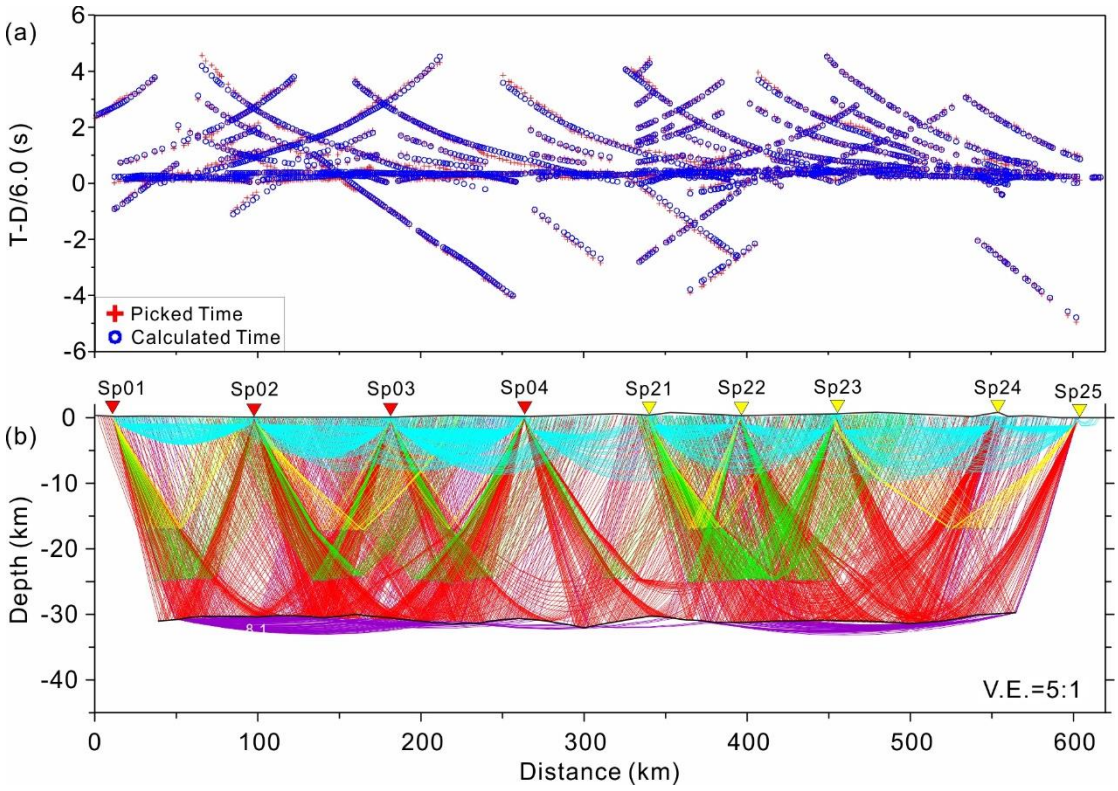

Figure 11. Travel time fitting and ray coverage for all shots. (a) Red crosses and blue circles indicate picked times and calculated times, respectively. (b) Cyan, yellow, green, red and purple rays represent Pg, P1, P2, PmP and Pn, respectively.

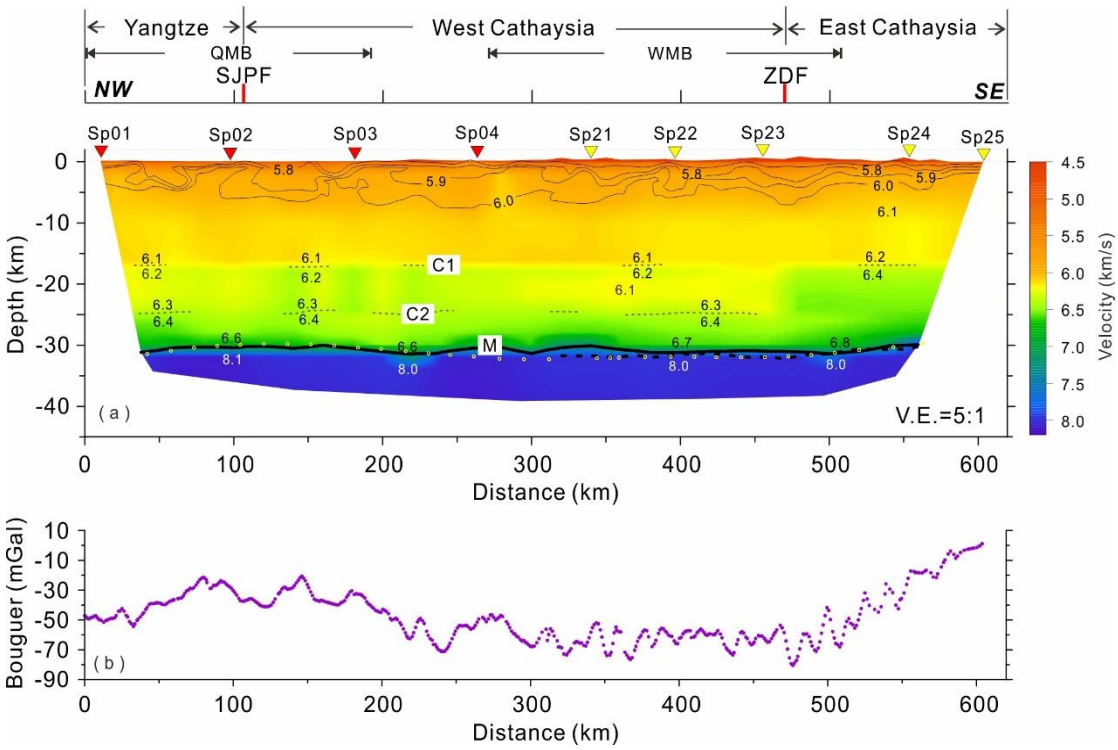

Figure 12. (a) Two-dimensional crustal P-wave velocity model along the Wanzai-Hui'an profile. The top panel shows the tectonic units and faults which are crossed by the profile: SJPF, Shaoxing-Jiangshan-Pingxiang fault; ZDF, Zhenghe-Dapu fault; QMB, Qinhang Metallogenic Belt; WMB, Wuyishan Metallogenic Belt. C1, C2 indicate intracrustal interfaces and C is the Moho discontinuity. The contour lines representing velocities less than 6.1 km/s in the upper crust are drawn from the finite differences-based 2D model obtained by Lin et al. (2020). (b) Bouguer gravity anomaly along the Wanzai-Hui'an profile.

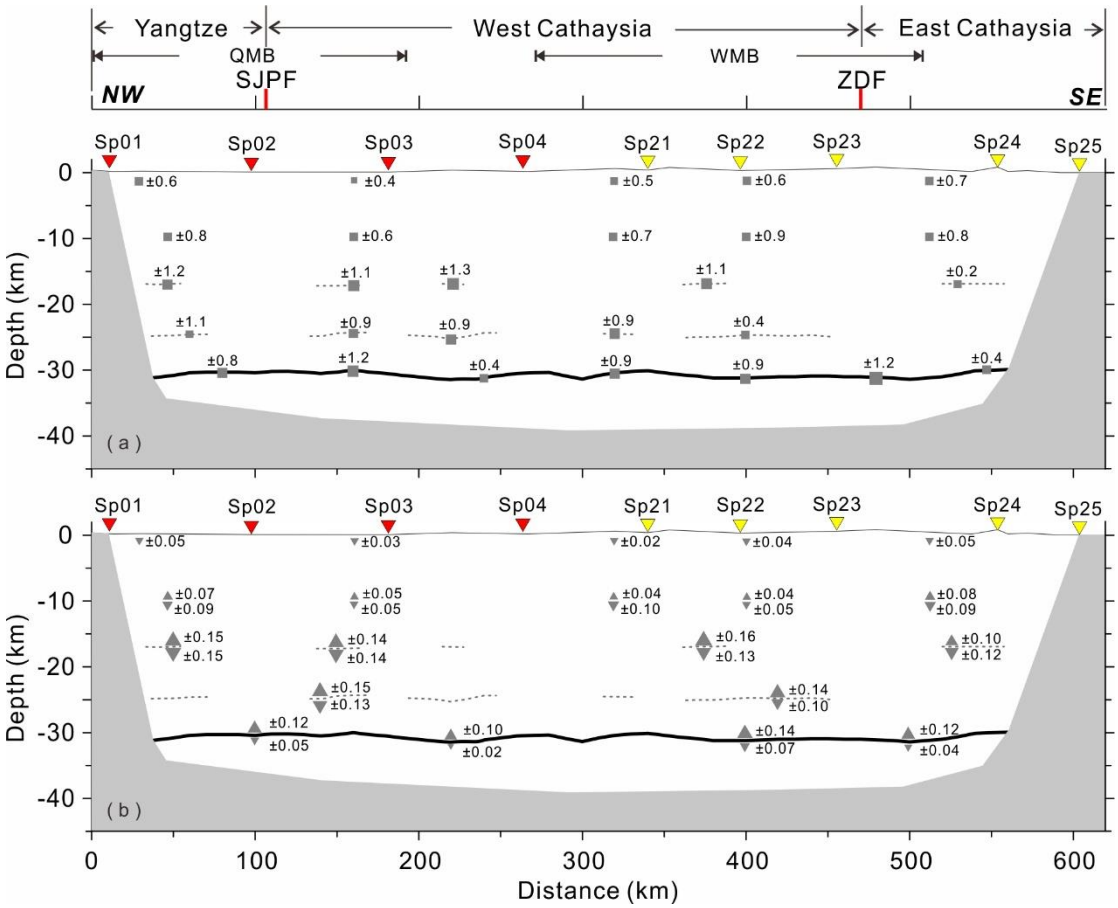

Figure 13. Resolution in velocity and depth of the 2D velocity model. (a) Uncertainties in layer limits (in km). (b) Uncertainties in seismic velocities (in km/s). The size of the symbols is relative to the absolute values. The dashed lines indicate the reflections within the crust, while the thick black line represents the Moho.

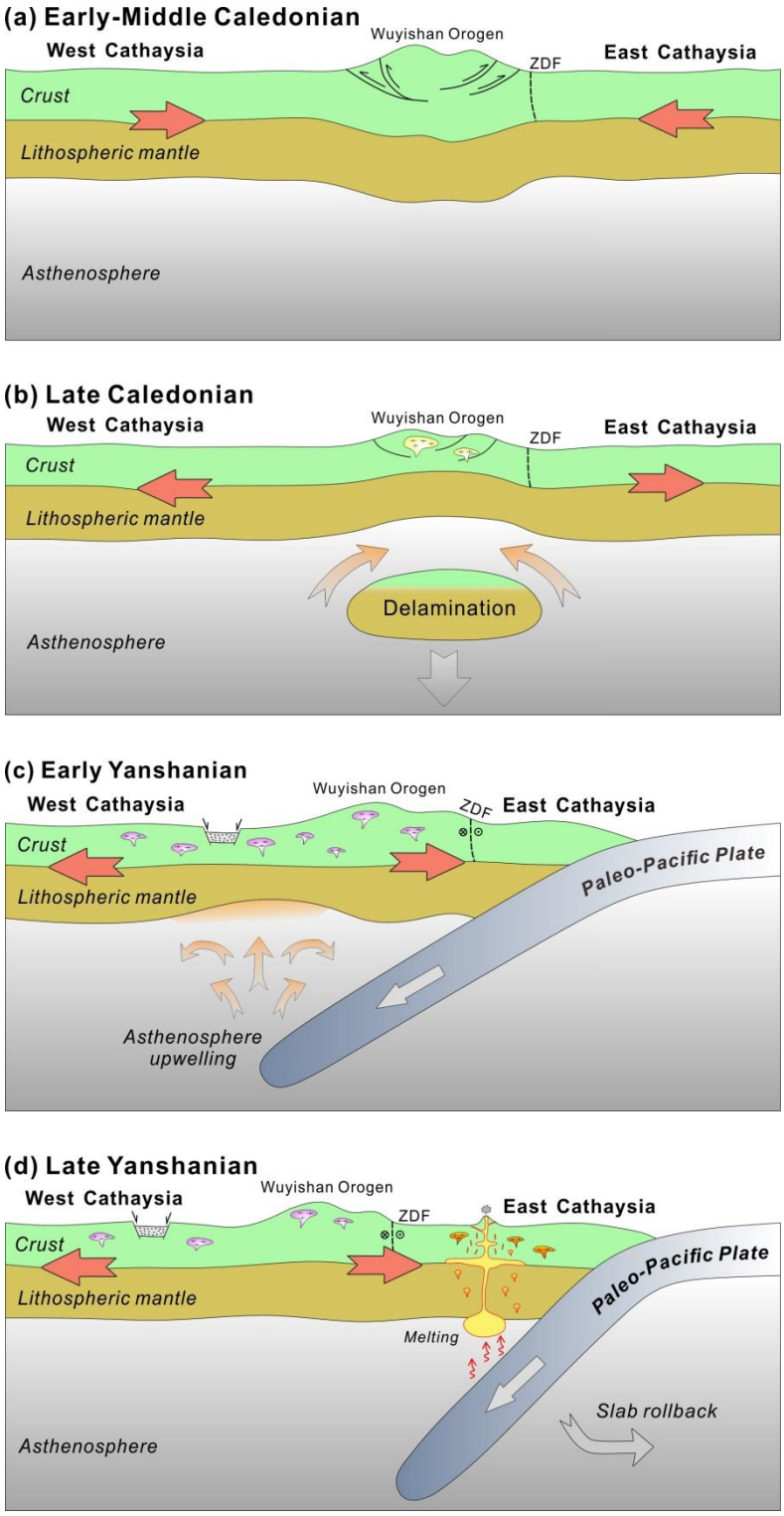

Figure 14. Schematic cartoon illustrating the tectonic evolution of the Cathaysia in SE China. (a) During the Early-Middle Caledonian (Ordovician), the crust and lithospheric mantle thickened due to the intracontinental orogeny of the South China block. (b) In response to the post-collisional extension during the Late Caledonian (Silurian), the

623 lower crust and lithospheric mantle collapsed. (c) During the Early Yanshanian
624 (Jurassic), the Paleo-Pacific plate started its subduction and the asthenosphere upwelling,
625 and then the back-arc extension resulted in the crustal material melting, which provided
626 the source to the widely distributed early Yanshanian (Jurassic) granite in West
627 Cathaysia. (d) During the Late Yanshanian (Cretaceous), continuous extension resulted
628 in the slab rollback of the Paleo-Pacific plate, and the dip of the slab increased, and
629 extensive melting and magma underplating caused the granite and volcanic rocks in East
630 Cathaysia.

631